A&A 434, 1005–1019 (2005)
DOI: 10.1051/0004-6361:20042217
© ESO 2005

Astronomy & Astrophysics

Edge-on T Tauri stars⋆

I. Appenzeller[1], C. Bertout[2], and O. Stahl[1]

[1] Landessternwarte, Königstuhl, 69117 Heidelberg, Germany
e-mail: O.Stahl@lsw.uni-heidelberg.de
[2] Institut d'Astrophysique, 98bis Bd. Arago, 75014 Paris, France

Received 30 March 2004 / Accepted 8 January 2005

Abstract. Using the UVES echelle spectrograph at the ESO VLT we obtained two-dimensional high-resolution (R = 50 000) spectra of the edge-on disk objects HH30*, HK Tau B, and HV Tau C. For comparison purposes we also observed with the same equipment both the classical T Tauri star HL Tau and the active late-type star LDN 1551-9. The spectra of all three observed edge-on disks consist of a T Tauri emission and absorption line spectrum with superimposed jet emission lines. Analysis of the spectra confirmed that the disks are completely opaque at visible wavelengths and that light from the central objects reaches us only via scattering layers above and below the disk planes. The central objects of our targets were found to be normal T Tauri stars showing moderate but different amounts of veiling of their photospheric spectra, indicating different accretion rates or evolutionary stages. We suggest that all classical T Tauri stars (CTTSs) show this observed morphology when viewed edge-on. Part of the jet emission from edge-on systems is directly visible to us in the forbidden lines as well as in Hα and He I, a finding which contradicts the present paradigm of a pure magnetospheric accretion origin for the formation of hydrogen and helium emission lines in moderately active CTTSs. From a comparison with those Taurus-Auriga CTTSs for which the inclination is reliably known, we conclude that the view angle of CTTS systems is one of the key parameters governing apparent Hα emission strength in the T Tauri class. We discuss the various possible formation regions for the Na I D lines and show that profiles similar to observed ones can be formed at the base of the disk wind.

Key words. stars: formation – stars: pre-main sequence – ISM: jets and outflows – planetary systems: proto-planetary disks – line: formation

1. Introduction

The development of high angular resolution imaging techniques in the optical, infrared, and millimetric bands has led to the discovery over the last decade of a number of resolved disks surrounding pre-main sequence stars (see the review by Ménard & Bertout 2002). These observations have confirmed the long held belief, based on indirect evidence, that young, solar type stars are often associated with disks (e.g. Appenzeller et al. 1984; Bertout et al. 1988).

While the circumstellar disks are known to contain the dust and gas needed for planetary systems to develop, their structure and evolution remain elusive. The relationship between these disks and the ubiquitously observed proto-stellar jets is a related question that also remains unsolved. A disk/jet connection is well established (e.g. Cabrit et al. 1990), but the origin of the jet and its driving mechanism remain topics of intense debate (see the review by Cabrit 2002).

Current models of gravitational collapse (Yorke & Bodenheimer 1999) predict that a quasi-hydrostatic accretion disk forms around the stellar embryo and grows in size and mass as the collapse proceeds, while feeding mass to the central star. However, the computed disk mass and size as the star approaches the main sequence both appear larger than observed, possibly because the role of the proto-stellar jet, of MHD instabilities, and of non-axissymmetric effects in carrying away angular momentum of the infalling matter is not taken into account in these simulations.

That the disk should grow radially because of outward angular momentum transport as its evolution proceeds appears nevertheless plausible, as already noted by Lynden-Bell & Pringle (1974) and more recently by Hartmann et al. (1998). It is perhaps not surprising, therefore, that the largest circumstellar disks are observed around young solar type stars that have become visible in the near-infrared and optical ranges, the T Tauri stars or Class II objects in the evolutionary scheme for solar-mass pre-main sequence objects originally devised by Adams et al. (1987) and extended by André et al. (1993).

Class II stars are surrounded by actively accreting disks (Bertout et al. 1988). The accretion onto the star is thought to be proceeding along the magnetic field lines of the stellar magnetosphere, which disrupts the inner disk regions. Class II objects also harbor jets, although less powerful ones than in previous evolutionary phases, such that they are often referred

⋆ Based on observations obtained with UVES at the ESO Very Large Telescope, Paranal, Chile (proposal No. 70.C-0041(A)).

Article published by EDP Sciences and available at http://www.aanda.org or http://dx.doi.org/10.1051/0004-6361:20042217

to as micro-jets. Because Class II objects are visible in the optical range, we can use the powerful technique of high-resolution optical spectroscopy to study them.

This technique has already been fruitfully used decades ago for the brightest young stellar objects (e.g. Mundt 1984) and, more recently, for several Orion proplyds (e.g. Henney & O'Dell 1999), the spectra of which are strongly affected by disk photo-evaporation caused by the intense UV radiation field from the Trapezium stars. But no high-resolution spectroscopy of the recently imaged edge-on disks surrounding nearby Class II objects has been available so far[1]. From the observed strong polarization it is known that only scattered light is reaching us from such objects. Hence, these objects are much fainter than ordinary T Tauri stars at the same distance, and large telescopes are needed to observe them with high resolution optical spectroscopy.

In order to learn more about the nature and evolutionary stage of the central objects of these disks and to derive information about the physical structure and properties of the observed proto-stellar disk-jet systems, we used the VLT UVES spectrograph to study the resolved edge-on disks surrounding the the central object of HH30 (in the following referred to as "HH30*") and the young stellar objects HV Tau C and HK Tau B. For comparison we also included in our UVES observing program the prominent classical T Tau star (CTTS) HL Tau and the presumed non-emission PMS star LDN 1551-9.

HH 30*, the central object of HH30, was discovered by Mundt & Fried (1983). Subsequently HH 30 and HH 30* were studied by many different authors from the ground (Mundt et al. 1987, 1990; Cohen & Jones 1987; Graham & Heyer 1990; Reipurth et al. 1993; Kenyon et al. 1998) and with the HST (Burrows et al. 1996; Wood et al. 1998; Watson & Stapelfeldt 2004). From a low-resolution optical spectrum Kenyon et al. (1998) estimated the spectral type of HH30* to be around M0.

HK Tau B was identified as an edge-on disk by Stapelfeldt et al. (1998) from HST and by Koresko (1998) from ground-based adaptive optics high-resolution images. A detailed description of the observed properties of this object can be found in Duchêne et al. (2003).

HV Tau C was discovered as the third component of the HV Tau system by Simon et al. (1992). After forbidden emission lines were observed in HV Tau C by Magazzu & Martin (1994), HV Tau C was included (as HH 233) in the Reipurth (1999) catalog of Herbig-Haro objects. The true nature of HV Tau C was clarified by Woitas & Leinert (1998) who showed that the observed IR flux could not be explained by an HH nebula but instead required the presence of a stellar central source. Finally, HV Tau C was identified as an edge-on disk by Monin & Bouvier (2000) using ground-based AO images and Stapelfeldt et al. (2003) using HST imaging.

[1] While this work was being revised, White & Hillenbrand (2004) published a spectroscopic study of a large sample of Taurus-Auriga YSOs, including the targets studied here. Our long slit spectra complement these data by providing additional information on the origin of emission lines in edge-on stars.

The comparison object HL Tau is listed as a CTTS in the PMS star catalog of Herbig and Rao (1972). Its optical spectrum, showing strong and broad emission lines superimposed on a veiled late-type photospheric absorption spectrum corresponding to ≈K7, has been described, e.g., by Herbig & Kameswara Rao (1972), Cohen & Kuhi (1979), and Basri & Batalha (1990). As in the case of our program objects, at optical wavelengths we receive only indirect light that is scattered towards us by the reflection nebula of HL Tau (Stapelfeldt et al. 1995), although the central object is directly visible at IR wavelength (Close et al. 1997). Radio observations of HL Tau have been interpreted as evidence for the presence of a massive dust and gas disk observed at an inclination of about 67° (Beckwith et al. 1990; Hayashi et al. 1993; Close et al. 1997), surrounded by an extended envelope. The star is also known to drive a prominent jet directed approximately perpendicular to the proposed disk (Mundt et al. 1990; Cabrit et al. 1996). All emission lines of HL Tau are broad and the forbidden lines are known to show complex, blue-shifted line profiles (Appenzeller 1983; Hamann 1994).

Our spectrum of the comparison object HL Tau confirms the spectral properties described in the literature cited above. A detailed discussion of HL Tau is outside the scope of the present paper; however, since our high resolution spectrum provides some improved information on this object, our new observations will be presented below together with our results on the edge-on disks.

The second comparison star, LDN 1551-9, located about 7′ NE of HL Tau, was identified (and classified as a K6 star) during a search for PMS stars in in the direction of the Lynds Dark Cloud 1551 by Feigelson & Kriss (1983). Although no line emission was detected, Favata et al. (2003) suggested that LDN 1551-9 is a PMS star of the Taurus star formation region on the basis of its X-ray flux. Our UVES spectrum of LDN 1551-9 shows a photospheric absorption spectrum corresponding to about M0 with narrow emission lines of Ca II H and K and an Hα absorption line that is partially filled in by emission. However, no Li I (1) 6708 Å absorption is detectable ($EW < 5$ mÅ). The radial velocity of the star differs by about 10 km s^{-1} from the CO velocity of LDN 1551 and the typical radial velocity of the Taurus PMS stars (cf. Table 2), so that we conclude that LDN 1551-9 is an active late-type star, but very likely not a PMS star. Nevertheless, its spectral type and the narrow absorption lines, showing no detectable rotational broadening, make this star well suited as a comparison star for our program objects.

The paper is organized as follows: Sect. 2 presents the observational details; in Sect. 3 we discuss the observed spectra; in Sect. 4 we discuss possible explanations for the observed spectral properties; and Sect. 5 presents our conclusions.

2. Observations and data reduction

Our data are based on observations carried out in service observing mode in December 2002 and January 2003 with UVES, the **U**ltraviolet and **V**isual **E**chelle **S**pectrograph at the Nasmyth platform B of ESO's VLT UT2 (Kueyen) on Cerro Paranal, Chile. For all observations the standard setting DIC1,

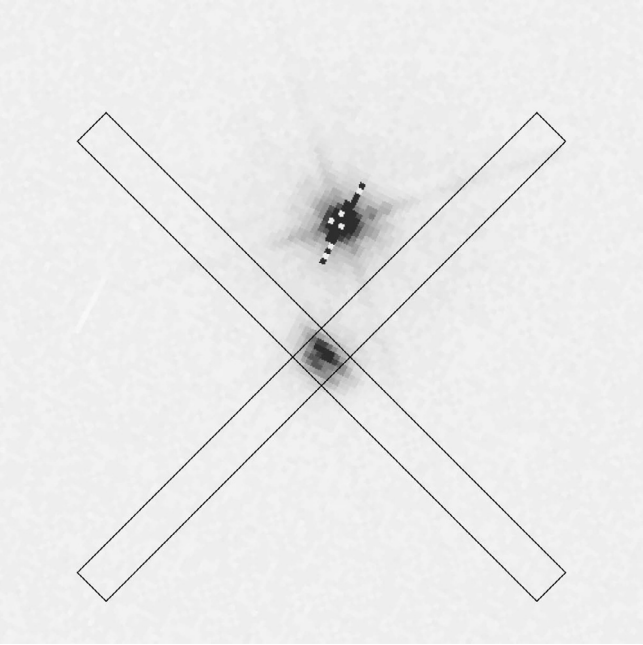

Fig. 1. HST archive image of HK Tau A and B with the positions and extent of the projected UVES red-channel spectrograph slits used for this study. The slit length is 11.″8. North is up and East to the left.

390+580, was used. The observed wavelength range extended from 3280 to 4490 Å in the blue channel and from 4726 to 6722 Å in the red channel, except for a gap from 5708 to 5817 Å due to the space between the two CCDs of the detector mosaic of the red channel. The projected slit width was 0.″8, resulting in a measured FWHM spectral resolution of about 50 000. The median FWHM seeing for the observations was 0.″83, but conditions varied significantly between the individual frames with extrema of 0.″53 and 1.″38.

The total integration times (between 5 min and 3.9 h) were split into individual exposures <50 min. Spectra were obtained for the program objects HH30* and HK Tau B with two different position angles of the projected spectrograph slit, with the slit oriented either parallel or perpendicular to the disk plane. In the case of HV Tau C only a spectrum with the slit parallel to the disk was obtained, since with an orientation perpendicular to the disk the slit would have passed too close to the bright main component HV Tau A/B of this triple system. In the case of the comparison object LDN 1551-9 (expected to be an unresolved star), the standard NS slit orientation was used. The slit was oriented parallel to the PA direction 140° for the comparison object HL Tau, i.e. approximately parallel to the extension of the dust and CO disks reported to be present at the position of HL Tau and perpendicular to the direction of the HL Tau jet (see e.g. Close et al. 1997; Mundt et al. 1990).

The pixel scales and slit lengths were, respectively, 0.″246 pixel^{-1} and 7.″6 in the blue and 0.″182 pixel^{-1} and 11.″8 in the red arm. As an example we present the contours of the "red" slit projected onto an image of HK Tau A and B in Fig. 1, while further information on the observations is listed in Table 1.

The observational data were reduced and two-dimensional spectra extracted using mostly standard ESO pipeline

Table 1. Some technical details of the observed spectra.

Object	Pos. angle	Nr. expos.	Tot. time (s)
HH 30*	120° (‖ disk)	6	14 056
HH 30*	30° (⊥ disk)	4	10 600
HK Tau B	135° (⊥ disk)	3	8460
HK Tau B	45° (‖ disk)	3	8460
HV Tau C	109° (‖ disk)	3	8640
HL Tau	140° (‖ disk)	1	300
LDN 1551-9	0°	1	300

software for UVES. An exception was the order-merger procedure where the ESO software did not produce satisfactory results, mainly because the very noisy edges of the echelle orders deteriorated the S/N in overlapping regions; therefore, the order merging was carried out using software developed at the LSW Heidelberg (Stahl et al. 1999). All spectral frames were converted to the same (heliocentric) wavelength scale. For the main targets, where several frames were available, we constructed mean spectra by calculating the median of the individual spectra.

In addition to the two-dimensional spectra we derived several sets of one-dimensional spectra by integrating along the direction perpendicular to dispersion with different integration limits. As discussed in detail in the following sections, these one-dimensional spectra were used to obtain information on the central stars and on various subcomponents of the observed objects. Since all objects are strongly reddened, the continuum S/N was in all cases <1 at the blue end of the spectral range, but reached values up to ≈60 at the red limit. Emission lines could generally be detected and evaluated for $\lambda > 3600$ Å.

3. The observed spectra

3.1. Basic spectral properties

In our UVES spectra all three edge-on disks show similar general spectral properties. Moreover, apart from the absence or weakness of permitted metallic emission lines (prominent in HL Tau), all our edge-on disks have spectra which qualitatively resemble that of HL Tau. In particular, all spectra include absorption lines of a late-type photosphere (with a spectral type around M0) and emission lines typical of CTTSs. Obviously, all observed edge-on disks contain CTTSs as central objects. Quantitatively, however, the edge-on disks do show some distinct differences when compared to other T Tauri stars:

i) all three edge-on objects have exceptionally strong forbidden lines relative to the continuum flux;
ii) as demonstrated in Table 3, the permitted emission lines are narrower than in HL Tau and other CTTSs and are (almost) undisplaced relative to the photospheric spectrum (cf. Table 2).

As an example we note that the *FWHM* of the Hα emission lines of our edge-on objects is <100 km s^{-1} in all three cases (with a mean of 61 ± 13 km s^{-1}), while for normal CTTS this value is in the range 100–500 km s^{-1} (see e.g., Hamann & Persson 1992). In contrast to many other CTTSs, our edge-on

Table 2. Observed heliocentric radial velocities of the photospheric absorption spectra (v_*), of the Hα emission line peaks (v_α), the He I emission line peaks ($v_{\rm HeI}$), the forbidden line peaks ($v_{\rm forbidden}$), the sharp absorption (or, in the case of LDN 1551-9, sharp emission) features of the resonance lines of Na I and Ca II ($v_{\rm Na-D}$ and $v_{\rm H\&K}$), and the velocity of the CO emission from the corresponding dark clouds ($v_{\rm CO}$). For the forbidden lines of HL Tau the velocities of the blue and the red peaks of the double-peaked profile are given. All values are heliocentric velocities in km s^{-1}. Where possible, statistical mean errors are included. If no error is listed the m.e. is about 2 km s^{-1}.

Object	Sp.Type	v_*	v_α	$v_{\rm HeI}$	$v_{\rm forbidden}$	$v_{\rm Na-D}$	$v_{\rm H\&K}$	$v_{\rm CO}$
HH 30*	K7	+21.5 ± 2.0	+20.3	+20.4	+19.8 ± 0.3	+20.6 ± 1.3		+19.0
HL Tau	K7	+20.7 ± 2.2	+99.6	+31.9	−173.5 ± 0.5	+20.7 ± 1.0	+22.4	+19.0
					+15.4 ± 1.2			
HK Tau B	M1	+17.1 ± 0.2	+12.5	+21.2	+12.1 ± 1.0	+18.8 ± 2.0	+17.9	+18.0
HV Tau C	M0	+20.3 ± 1.2	+12.5	+24.7	+12.2 ± 2.4	+16.8 ± 0.5	+17.5	+18.7
LDN 1551-9	M0	+31.0 ± 0.5					+29.6	+19.0

Table 3. Observed average FWHM (in km s^{-1}) of the observed emission lines (except for the complex forbidden lines of HL Tau, for which we give the full width at zero intensity). If no error is listed the m.e. is ≤10% of the measured value.

Object	Hα	He I	Na I (D)	Ca II H&K	Forb. Lines
HH 30*	50	35	33	?	25 ± 1
HL Tau	267	170	149	130	≈300
HK Tau B	37	34	34	25	33 ± 3
HV Tau C	96	58	36	43	51 ± 1

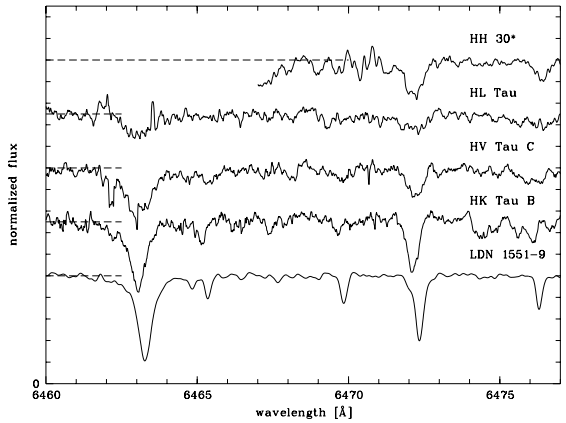

Fig. 2. Section of the photospheric spectrum of two of the edge-on disks and of the two comparison objects. The four spectra have been normalized to the same continuum level of 1.0. To avoid overlapping, the zero levels have been shifted vertically by 0.5, 1.0, 1.5, and 2.0, respectively, for HK Tau B, HV Tau C, HL Tau, and HH 30*. The 6460–6467 Å section of the HH 30 spectrum was affected by instrumental defects and therefore omitted.

disks show no, or only very weak, displaced or broad forbidden-line components, and all emission lines exhibit simpler and more symmetric profiles than normally observed in CTTSs.

As shown by Fig. 2, the spectra of the three edge-on objects are veiled. The amount of veiling – defined by the ratio *[excess flux]/[photospheric flux]* and estimated from the rest intensities of the strongest photospheric absorption lines and by comparing the line strengths with those observed in LDN 1551-9 in the red spectral range (around 6400 Å) – is about 0.2 for HK Tau B and approximately 0.5 for HH30* and HV Tau C. The different amounts of veiling may indicate that the central objects of our targets cover a range of PMS evolutionary stages or at least a range of accretion rates.

For all three edge-on objects the veiling is weaker than in HL Tau, which again indicates either more modest disk accretion rates or a more advanced evolutionary stage of the central stars. Given the moderate veilings of our target stars, the large equivalent widths of their emission lines (Table 4) is unexpected.

Table 4. Observed equivalent widths (in Å) of selected strong emission lines.

Object	Hα	[O I]λ6364	[S II]λ6716
HH 30*	454 ± 15	100.2 ± 1.5	104.5 ± 0.2
HL Tau	78 ± 0.2	1.3 ± 0.2	4.5 ± 0.2
HK Tau B	9.6 ± 0.2	0.4 ± 0.1	0.9 ± 0.2
HV Tau C	49.2 ± 0.2	7.8 ± 0.1	6.3 ± 0.1

3.2. The photospheric absorption spectra

As already noted, all our edge-on disk spectra contain absorption lines with line profiles and relative line strengths that agree well with those of late-type stellar photospheres. From comparing the relative line strengths with MK standard star spectra observed at a similar spectral resolution and by evaluating the shapes (but not the absolute strength, which may be affected by veiling) of the TiO-Bands, we estimated the approximate spectral types listed in Table 2. The luminosity classes appear to be about IV but cannot be determined precisely from our spectra since they show veiling effects and since we have a sufficient continuum S/N only in the red where few diagnostic lines are available. Because of the limited wavelength range usable for classification, the spectral types listed in Table 2 cannot be regarded as more accurate than those derived from lower resolution spectra.

As again illustrated by Fig. 2, the photospheric line profiles of all our three edge-on objects are narrow. In the case of HK Tau B, the low veiling allows us to derive an upper limit for a possible rotational broadening of $v \times \sin i < 10$ km s^{-1} from

the weak photospheric lines. The profiles observed in the spectra of HH30* and HV Tau C are consistent with such low $v \times \sin i$ values as well. But, since only the *intrinsically* broad strong lines could be detected in these spectra, the observational upper limit for rotational broadening is as high as 20 km s^{-1}. These limits demonstrate that no rotation is observed to be higher than normally expected for CTTSs, which gives further support to the normal CTTS character of the central objects of the edge-on disks.

3.3. Wind and jet emission lines

In T Tauri stars the winds and outflows, which often are collimated towards the rotation axes and then called "jets", are known to produce extended emission regions dominated by low-ionization forbidden emission lines. In the spectra of all our three edge-on disks and in the spectrum of HL Tau, all expected lines of [N II], [O I], [S II], and [Fe II] were clearly detected. HH30*, HV Tau C and HL Tau also showed [N I]$\lambda\lambda$ 5198, 5200 emission while [O II]$\lambda\lambda$3726, 3729 and [O I]λ5577 could be reliably detected only in HH30* and HV Tau C. The relative strength of the [O II] doublet components indicate rather high electron densities for the volume producing these lines ($n_e > 10^5$ for HH30* and $\approx 10^4$ for HV Tau C).

As illustrated by Figs. 3, 4, and 7, extended jet emission was observed in the two spectra which were taken with the spectrograph slit oriented perpendicular to the (projected) disk plane (i.e. the spectra PA = 30° of HH30* and PA = 135° of HK Tau B). On the other hand, extended forbidden-line emission was *not* detected in any of the other spectra, which all were taken with the slit parallel to the (projected) disk planes. In fact, the forbidden-line emission region was unresolved, i.e. the *FWHM* extent of the emission region was not larger than that of the seeing profile, in all our edge-on disk spectra taken with a disk-parallel slit. This finding is consistent with the result of Burrows et al. (1996), who found for the HH30 jet a width at the base ≤20 AU, which is below the resolution of our ground-based observations. The continuum emission in the disk-parallel spectra always showed an extension significantly larger than the forbidden-line emission. Obviously, most the forbidden-line flux that entered the spectrograph slit reached us directly from an unresolved emission region above the disk while the continuum emitted by the central star is scattered towards us by an extended and resolved dusty region.

As pointed out (e.g.) by Takami et al. (2003) line emission regions slightly off-set from the center of the continuum emission can in theory also be produced by unresolved, very close binary components. However, for our edge-on object a jet origin of the observed forbidden-line emission appears much more plausible.

For each of the three edge-on program objects all forbidden lines (including the [Fe II] lines) were found to show identical or qualitatively similar line profiles in the one-dimensional mean spectra averaged over the two slit orientations. On the other hand, these profiles differ between the different targets.

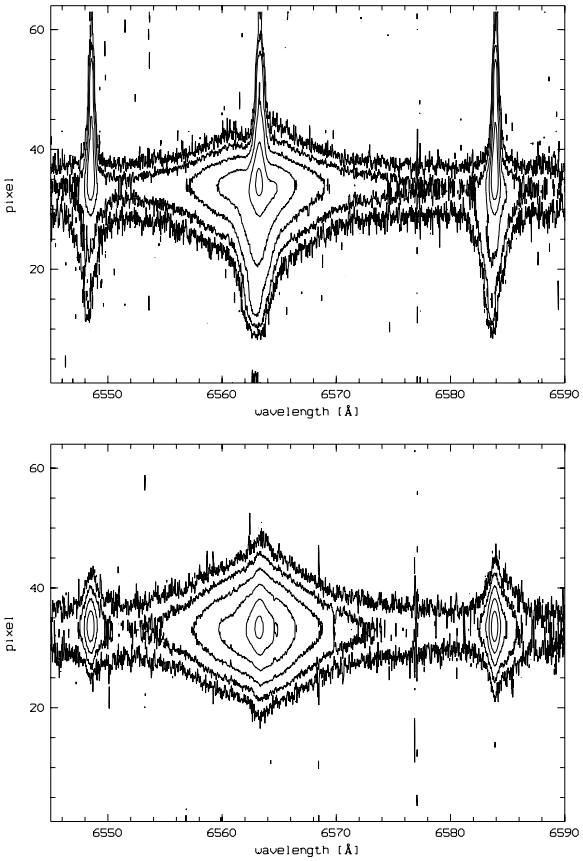

Fig. 3. Contour diagrams of the 2D spectra of HH30* **a)** with the slit oriented parallel to the jet, and **b)** with the slit parallel to the disk, showing the Hα and the adjacent [N II] lines. Between two contours the intensity changes by a factor of 3.16 (=$\sqrt{10}$).

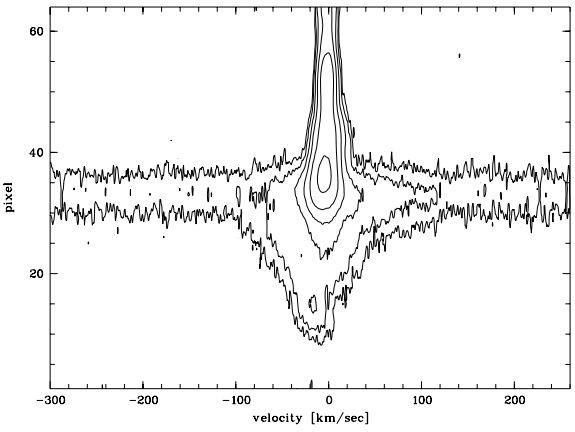

Fig. 4. Contour diagrams of the 2D spectrum of HH30* showing the [S II] 6717 Å line with the slit oriented parallel to the jet. Between two contours the intensity changes by a factor of 3.16 (=$\sqrt{10}$). The zero-point of the velocity scale corresponds to the object's adopted systemic velocity of +20.1 km s^{-1}.

3.3.1. HH30*

In the case of HH30* the forbidden-line profiles are dominated by narrow cores with a heliocentric peak radial velocity of +19.8 ± 0.3 km s^{-1}. This value is (within the error limits) in agreement with the weighted mean of all velocities measured

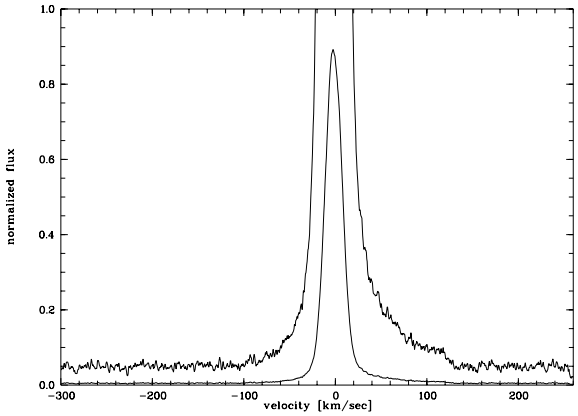

Fig. 5. Profile of the [S II] 6717 Å line of HH30*, plotted at two different vertical scales (differing by a factor 10) to show the two different components. The zero-point of the velocity scale corresponds to the object's systemic velocity.

in the integrated spectrum of HH30* (20.1 km s^{-1}), which was adopted as the systemic velocity of HH30*. Underlying the narrow cores, the forbidden-line profiles include much weaker and redshifted broad components (*FWHM* > 100 km s^{-1}, see Fig. 5).

The resolved extended emission in the direction of the prominent HH30 jet (i.e. towards PA ≈ 30°, cf. Burrows et al. 1996) shows only the narrow profile components, which are slightly redshifted by about 3.0 km s^{-1} (see Figs. 3 and 4). The weaker and less extended emission towards PA ≈ 210° (usually referred to as the "counter-jet") shows somewhat broader line profiles that are blue-shifted by about 13.0 km s^{-1} relative to our adopted systemic velocity. If these small velocity shifts are due to a tilt of the jet, they would indicate that – contrary to the expectation from the morphology – the counter jet is approaching us, while the north-northeast emission region is receding. However, the small differences in the systemic velocity show that any tilt, if present, is very small. Since the HH30 jet is known to be slightly curved (cf. Burrows et al. 1996), the observed velocity shifts may simply reflect small deviations from a linear flow.

The narrow (jet) line profile component is also visible in Hα (cf. Fig. 3 and 6) and in the He I emission lines. As illustrated by Fig. 3 (and Fig. 6), the Hα line profile also includes a very broad component (extending to at least ±340 km s^{-1} from the line center) at the position of the continuum source (but not in the jet). Moreover, in the area covered by our spectrograph slit the jet and the counter jet show nearly the same Hα flux, while the forbidden-line flux is very different.

3.3.2. HK Tau B

As illustrated by Fig. 7, our HK Tau B spectrum, taken with the slit perpendicular to the disk, shows extended forbidden-line emission directed towards PA 315°. In this direction the slit passes unfortunately close to the position of the brighter star HK Tau A, which is known to show exceptionally strong Hα emission (Kenyon et al. 1998). Therefore, the Hα emission from the HK Tau B jet is contaminated by straylight from

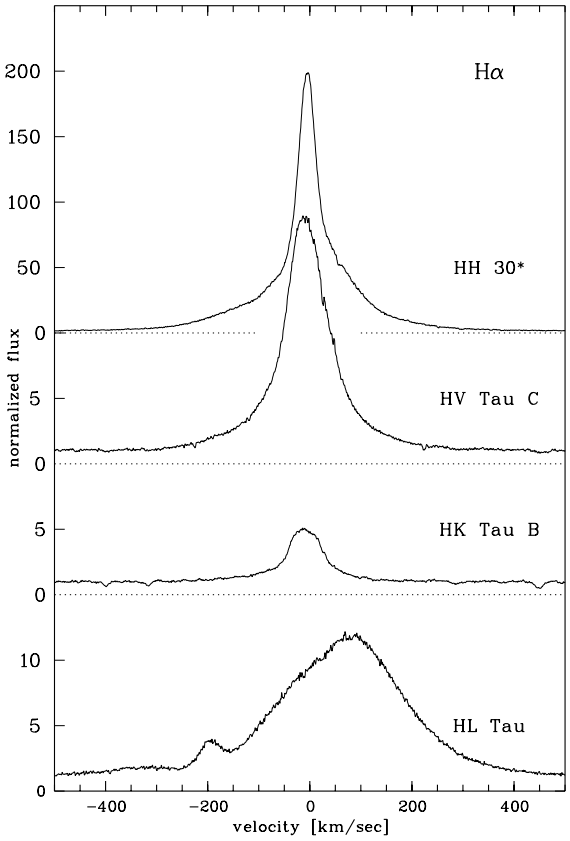

Fig. 6. Profile of the Hα line of our three targets and of the comparison CTTS HL Tau. The zero-point of the velocity scale corresponds to the objects' systemic velocity. The sharp absorption at about +50 km s^{-1} is an artefact.

the Hα line of HK Tau A. HK Tau A may also contribute to the observed forbidden line flux observed below the disk of HK Tau B, but the observed intensity distribution perpendicular to the dispersion direction rules out any possibility that all the extended emission is due to straylight from HK Tau A. The observed jet emission of HK Tau B is again dominated by a narrow and almost unshifted ($\Delta v \leq 5$ km s^{-1}) line component, while an underlying broader component could not be detected. However, since the forbidden lines are weaker in HK Tau B and since the photospheric spectrum (less veiled) is more prominent, a broad component as weak as in the case of HH30* would not be detectable in our HK Tau B spectra.

3.3.3. HV Tau C

In HV Tau C the forbidden lines are somewhat broader than in HH30* and HK Tau B (see Table 3), and some line profiles appear slightly asymmetric, with the red wing slightly more extended than the blue wing. A slight asymmetry is most pronounced at the [N II] lines, while [S II]λ6716 is practically symmetric. As illustrated by Fig. 8, the base of all forbidden lines of HV Tau C has about the same redshift. Hence the asymmetry appears to be caused by a shift of the emission peak towards shorter wavelengths. A possible explanation of the asymmetry could be the presence of two profile components, as observed in HL Tau (Fig. 9), but with a velocity separation that is small

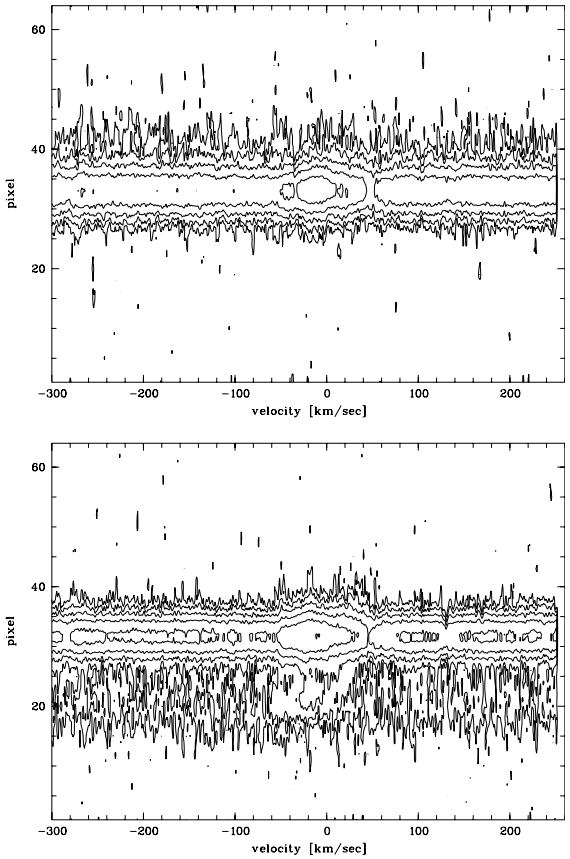

Fig. 7. Contour diagrams of the 2D spectra of HK Tau B showing the region of the [S II] 6717 Å line, **a)** with the slit oriented parallel to the jet, and **b)** with the slit parallel to the disk. Between two contours the intensity changes by a factor of 2. The zero-point of the velocity scale corresponds to the object's systemic velocity.

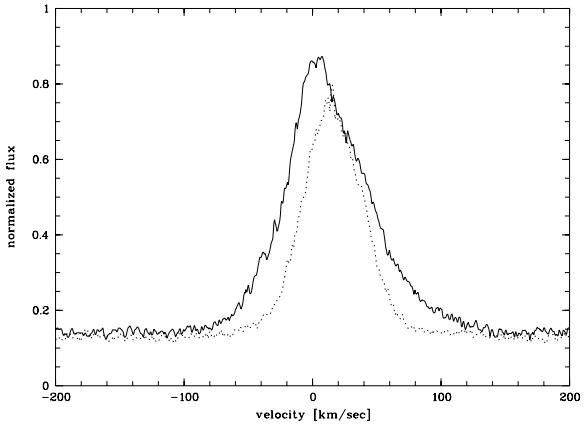

Fig. 8. Line profiles of the [N II] 6583 (solid line) and [S II] 6717 Å lines in the spectrum of HV Tau C. The zero-point of the velocity scale corresponds to the object's adopted systemic velocity.

compared to the line width in the case of the (almost) edge-on disk object HV Tau C.

3.3.4. HL Tau

Our (presumably non-edge-on) comparison object, HL Tau, has been known to have blue-shifted and, in some cases,

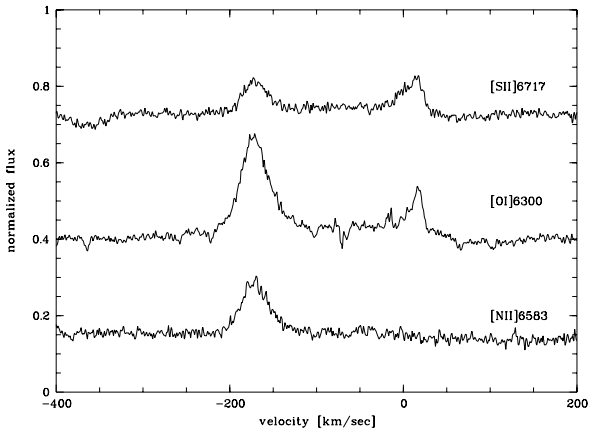

Fig. 9. Line profiles of the [N II] 6583, [O I] 6300, and [S II] 6717 lines in the spectrum of HL Tau. The abscissa gives the heliocentric radial velocity.

double-peaked forbidden-line profiles (Appenzeller 1983; Hamann 1994; Hirth et al. 1997). This is confirmed by our new observations with improved accuracy. As shown by Fig. 9 and Table 2, one forbidden line component is blue-shifted by 194 km s^{-1} relative to the photospheric spectrum, while the other component shows almost the same radial velocity as both the absorption spectrum and the sharp resonance line absorption components of HL Tau. Appenzeller et al. (1984) and others pointed out that such profiles are not unexpected for disk-jet systems seen at intermediate inclinations. As illustrated by Fig. 9, the relative strength of the two profile components varies greatly between the different forbidden lines, indicating that the two components originate in different volumes, (as also observed in some other CTTSs, see Hirth et al. 1997). This is confirmed by our two-dimensional HL Tau spectrum (taken with the slit parallel to the projected disk), where the emission region producing the blue-shifted peak is unresolved, and thus probably originates in a directly observed narrow jet intersected by the slit, while the region producing the red peak is extended and shows about the same angular extension as the continuum.

It seems plausible that the low-velocity emission originates in a rarefied extended emission region, as proposed for other CTTSs with similar profiles by Kwan & Tademaru (1988). The slight blue-shift (≈5 km s^{-1} relative to the photospheric spectrum) could be caused either by a slow outflow or by scattering in a slowly moving medium. That the two components of the [S II] line are of similar strength in Fig. 9, while the [S II]λ6731 profile published by Hirth et al. (1997) is dominated by a much stronger high-velocity component is probably due to our slit orientation approximately perpendicular to the jet, which suppresses much of the jet emission.

3.4. Circumstellar spectral features

The CTTS disks are known to be essentially composed of relatively dense cool and dusty gas, so we expected to see spectroscopic signatures for the disks mainly in the profiles of the low-ionization resonance doublets of Ca II (H & K) and Na I (D). The observed features were in all cases well separated from the

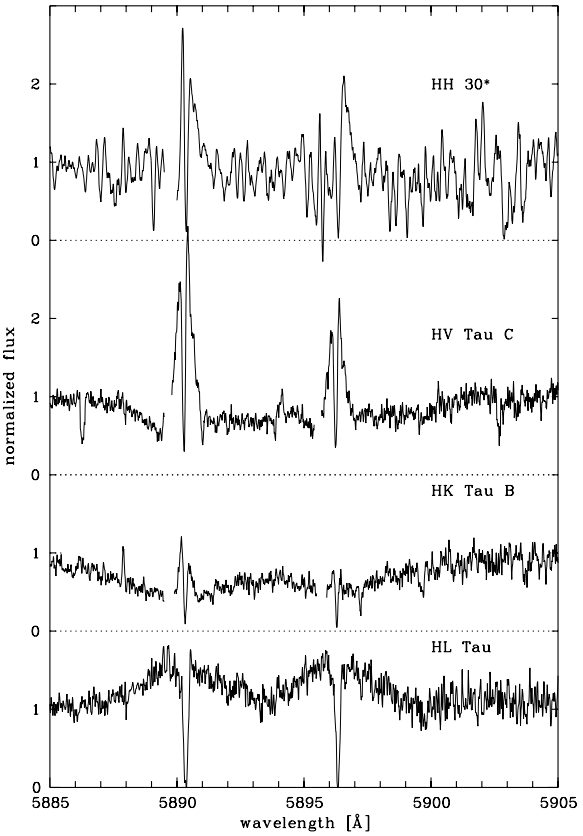

Fig. 10. Na I (D) resonance line profiles in the spectra of HH 30*, HV Tau C, HK Tau B, and HL Tau.

corresponding telluric lines because of the high resolution of the UVES spectra and the significant systemic radial velocities of all observed objects.

All three edge-on objects and HL Tau show the Ca II and Na I resonance doublets in emission, although the lines are surprisingly weak in HH30*. In the edge-on disks the resonance line emission profiles are generally narrow with *FWHM* values similar to those of the forbidden lines and the He I emission lines (cf. Table 3 and Fig. 10). An exception may be Ca II H & K of HH30*, where weak broader emission lines appear to be present. However, the S/N of our spectra did not allow us to reliably measure the widths of these very weak features. The non-edge-on system HL Tau shows much broader and stronger (relative to the continuum) Ca II and Na I resonance emission. In Fig. 10 we compare the Na I (1) emission profiles of the edge-on disks with those of HL Tau. The region from which the resonance line emission is received has about the same angular extension as the continuum in all objects, so that the directly visible parts of the jets do not seem to contribute to resonance line emission. Most of the Na I emission must originate near the star, whether in the central region of the disk or at the base of the jet, and is (like the continuum) obviously scattered towards us by matter above and below the disk plane. A more detailed discussion of the origin of this emission will be given in Sect. 4.

In addition to the emission we found at all Na I lines, and at all Ca II resonance lines observed with sufficient S/N, very narrow absorption components with radial velocities agreeing well with those of the photospheric spectra (cf. Table 2). For all three edge-on objects the profiles of these absorption components do not deviate significantly from the instrumental profile ($FWHM \approx 6$ km s^{-1}). In the case of HL Tau the width of the absorption component corresponds to about twice the instrumental profile. For HH 30*, HK Tau B (and HL Tau) the narrow Na I absorption components reach well below the level of the adjacent continuum and almost to zero intensity, indicating that the absorption affects practically all light reaching us at this wavelength. Hence, the absorption must at least in part be of interstellar or circumstellar origin. Because of the absorption strength and the excellent agreement of the observed velocities with the objects' systemic velocities, a circumstellar origin appears most plausible. Absorption could, in fact, take place in the same cool dusty matter that scatters the light from the central objects and the inner disks towards us.

In case the absorbing matter were related to the disks, our 2D spectra taken with the slit parallel to the disk might well contain information on the disk rotation. If the absorbing matter were orbiting at 100 AU around a central object of one solar mass we would expect an orbital velocity of about 3 km s^{-1}, which is within reach of UVES spectra. Therefore, we checked our 2D spectra for a possible tilt of the sharp absorption component, but we found no evidence for rotation. The most accurate measurement (Na I D of HV Tau C) resulted in a (non-significant) tilt of 0.48 ± 0.26 km s^{-1} arcsec^{-1}. Since seeing tends to smear possible rotational signatures in our ground-based spectra, our result does not rule out rotational disks velocities of a few km s^{-1} as estimated above.

4. Interpretation and discussion

4.1. Forbidden line emission

As pointed out above, in all three edge-on objects there is clear evidence that the narrow forbidden line components are emitted by jet flows that are seen directly above and below the disks. The small line width of the narrow forbidden-line components and the small velocity shifts are readily explained by the fact that in the edge-on objects the gas in the jet and counter jet is moving perpendicular to the line-of-sight within a few degrees. The weaker, broad, and shifted components observed from the same extended area from which we observe the continuum flux can possibly be explained by additional light from the jets scattered towards us above and below the disk by the same material that scatters the light from the central star. As the jet plasma moves supersonically with a significant line-of-sight velocity component relative to the scattering medium, with most of the jet material moving away from the scattering layer, such radiation is expected to show significant line broadening and a velocity shift, as was indeed observed.

The weakness of the forbidden-line emission from the counter-jet of HH 30*, in spite of strong Hα emission, may indicate that this radiation is produced in a relatively dense medium. Either the counter jet is moving into a much denser environment, which could also explain the smaller extent, or we see in Hα light coming from a different emission region that is scattered in our direction.

4.2. Wind contribution to Hα and He I lines

Current models for CTTSs attribute Hα emission to the magnetospheric accretion region in all but the most extreme CTTSs (Muzerolle et al. 1998, 2001). Before the magnetospheric accretion paradigm became consensual, a number of other possible origins for Balmer line emission had been discussed in the literature, for example, strong winds (e.g., Kuhi 1964; Hartmann et al. 1982), deep chromospheres (e.g., Calvet et al. 1984), or disk boundary layers (Basri & Bertout 1989). Because they can form in a large range of conditions, it is particularly difficult to disentangle the contributions to the Balmer lines from all possible emission regions. As we have seen above, the particular geometry of edge-on objects allows us to isolate the contribution of the jet to forbidden emission. The Hα and He I lines share many similarities with the forbidden lines in edge-on objects, and can be understood in the same way. In particular, the narrow Hα and He I emission cores can be understood as jet emission seen above and below the disk, so they provide direct evidence that the jet contributes to the formation of strong permitted emission lines in these objects.

Since we have noted above the strong similarities between edge-on stars and other CTTSs, the finding that the jet contributes to Hα suggests that emission from the CTTS outflow is an essential ingredient of Hα emission even in moderately veiled CTTSs. This contrasts with current magnetospheric accretion models, and suggests that the view angle under which a given CTTS is seen partly determines the properties of its emission lines.

In order to test this new hypothesis, we now investigate a cross-section of Taurus-Auriga CTTSs for which (a) precise photometric periods and radial velocities and (b) simultaneous determinations of Hα equivalent widths and veiling are known. This sample is given in Table 5, where the star name and Herbig and Bell catalog number are given in Cols. 1 and 2. The photometric periods and radial velocity measurements, originating from a compilation of the literature by J. Bouvier (priv. comm.), are given in Cols. 3 and 4 respectively. The photospheric radius, derived as in Strom et al. (1989), is listed in Col. 5. The view angle inferred from the previous quantities is given in Col. 6, while Cols. 7 and 8 list the Hα equivalent widths and veiling values in the red spectral range, as determined by Alencar & Basri (2000) from high-resolution Hamilton spectrograms. To these 12 stars, we add the 3 edge-on TTSs, for which the inclination angle is close to 90°. Their EWs are given in Table 4.

In order to meaningfully compare the Hα equivalent widths, we computed their value at zero veiling using the procedure given in Alencar & Basri (2000). By doing this, we presumably eliminated the effect of varying mass accretion rates in different stars on their line emission strengths. We then constructed a histogram of the average corrected EW(Hα) in equal cos *i* intervals. Figure 11 shows the result for a 3-bin histogram, with bins containing 6, 5, and 4 stars, respectively. A strong correlation of the average corrected EW(Hα) with view angle is apparent, readily understood in the framework of the interpretation discussed above; as the view angle increases, the jet contribution to the Hα flux becomes more and more apparent as a separate emission region, thus driving the equivalent width value up. Note that the correlation is not due to the particular distribution used in Fig. 11, as we found that the correlation remains strong even with 5 bins.

Table 5. Properties of Taurus-Auriga CTTSs with known inclination angles and simultaneous *EW*(Hα) and veiling determinations. Details and references are given in the text.

(1) Star	(2) HBC	(3) $P_{\rm rot}$ [d]	(4) $v \sin i$ [km s^{-1}]	(5) R [$R_\odot$]	(6) i [°]	(7) EW(Hα) [Å]	(8) v
BP Tau	32	7.6	7.8	2.2	32	48.6	0.5
DE Tau	33	7.6	10	1.78	57	66.5	0.9
T Tau	35	2.8	20.1	4.2	15	63.1	0.1
DF Tau	36	8.5	16.1	3.45	50	61	1.8
DG Tau	37	6.3	21.7	2.8	58	60.5	2
DK Tau	45	8.4	11.4	2.7	44	16.7	0.4
GG Tau	54	10.3	10.2	2.5	56	40.2	0.3
GK Tau	57	4.65	18.7	2.37	46	34	0.2
DL Tau	58	9.4	16	2.92	78	110.2	1.9
AA Tau	63	8.2	11.3	1.94	69	14.2	0.3
DN Tau	65	6.0	8.1	1.93	30	15.7	0.1
RW Aur	80	5.3	17.2	3.00	37	45.9	2.0

While a detailed investigation of inclination effects on CTTS spectral lines is beyond the scope of this work on edge-on stars and will be the topic of a forthcoming paper, Fig. 11 clearly demonstrates that the view angle of CTTSs is one of the parameters determining their emission properties. The two parameters now known to play a role in CTTS line emission are the mass accretion rate and the view angle of the system. The dispersion of EW(Hα) within the single bins of Fig. 11 indicates that (at least) a third yet unknown parameter must also play a role in the complex CTTS line emission process. To conclude this section, we note that since the equivalent widths of Hα and forbidden lines vary with inclination, physical properties that are usually derived from these quantities, such as the wind mass-loss rate, must be viewed with some caution.

4.3. Other permitted lines: Na I D emission

The interpretation of other permitted lines observed from the spatially extended scattering region above and below the disks is more difficult. Using the HST images and the known distance of the Taurus association (139 pc, Bertout et al. 1999), we find that most of the light reaching us is scattered towards us at heights of about 15 AU (HK Tau B), 35 AU (HV Tau C) and 55 AU (HH 30*). In all three cases most of the scattered light is observed within a projected angle of ±45° of the pole direction. To connect these observational facts to the actual scattering geometry requires some knowledge of disk geometry, distribution of the scattering matter, and of the scattering asymmetry parameter of the dust grains involved.

4.3.1. Scattering from an extended envelope?

The spectroscopic results described above obviously contain information on the scattering geometry. One of our main

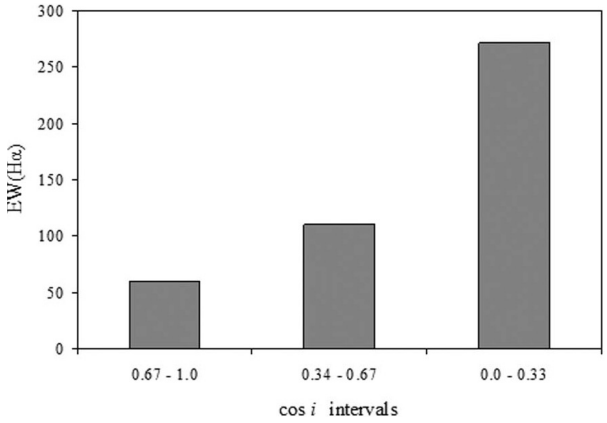

Fig. 11. Histogram showing the CTTS Hα equivalent width at zero veiling averaged over the stars included in 3 bins of equal cos *i* intervals spanning the full range of view angles. A similar result is found when distributing the stars over 5 bins.

findings has been the exceptionally narrow Na I resonance emission lines compared, e.g., to HL Tau. As pointed out in Sect. 3.4, these lines were not detected in the parts of the jets observed directly above and below the disks, which means that the outer regions of the jets do not significantly contribute to these lines. Moreover, the angular extent of the area from which these lines are observed seems to correspond closely to that of the stellar continuum. Thus the Na I emission apparently originates in the central part of the edge-on systems in the vicinity of the central stars. Since significant emission in neutral resonance lines is expected from volumes of cool intermediate-density gas, we expect the innermost regions of the system to be the main source of Na I resonance line emission.

In the co-rotating magnetospheric accretion models generally assumed today, the inner disk, the accretion flow, and the base of the jet rotate approximately with the Keplerian circular velocity of the inner edge of the disk, so that we expect line emission from these regions to show rotationally broadened profiles. Narrow profiles are expected only if these regions are viewed perpendicular to the rotational velocities, i.e., essentially pole-on. Obviously this would be the case if the matter above and below the disk, which scatters the radiation into our direction, is located close to the disk symmetry axis. Such a geometry would also be consistent with the narrowness of photospheric lines observed.

Scattering by matter vertically above and below the disk center is to be expected if isotropically scattering dust grains are involved and if (as predicted by protostellar model computations) the disks are surrounded by dusty, but optically thin remnant protostellar envelopes, or if the disk's matter density decreases slowly in the vertical direction. If the scattering material is of protostellar origin and is still in free fall, this would result in a small blueshift of the scattered light. However at the vertical distances considered here the corresponding velocities would be no more than a few km s^{-1} and would thus not be detectable in our spectrograms.

The suggestion that edge-on disks could be effectively seen close to pole-on not only appears counterintuitive but also apparently contradicts current scattering light models. In the last few years, edge-on T Tauri disks have been modeled assuming α-disks irradiated by their central stars (D'Alessio et al. 1998, 1999, 2001) or using models with assumed parameterized radial and vertical density distributions (see e.g. Wood et al. 1998; Watson & Stapelfeldt 2004). Theory, as well as observations, suggests that grain growth does occur in the T Tauri disks (see e.g. D'Alessio et al. 2001). Disk matter could therefore show much stronger forward scattering properties than normal interstellar dust. In models assuming such strongly forward scattering grains, the volume scattering the radiation from the disk center into our direction will be shifted towards us, and thus we will view the disk center at an intermediate angle, or under extreme conditions, more or less edge-on. Such models are able to produce intensity maps that agree reasonably well with observed images and spectral energy distributions of edge-on systems.

However, as discussed by Watson & Stapelfeldt (2004) the many free parameters of such models are not well constrained by comparisons with the observed energy distributions and continuum light distributions. Observations can be fitted reasonably well with a wide range of dust properties and geometric parameters. Furthermore, these models were developed chiefly for modelling the disk near-infrared continuum emission and often do not take into account the protostellar envelope and outflows that are associated with these disks. Stapelfeldt et al. (2003) indeed had to assume the existence of a spherical envelope, in addition to the disk, to model the *I* band image of HV Tau C. Such an additional envelope is not needed to reproduce the *K* band image, as it maps a lower temperature region. The possibility that dust contained in the envelope and jet regions affects the scattering process in such a way that edge-on objects are effectively seen from regions close to their rotation axis, as far as their optical light is concerned, may thus not be as implausible as seems at first. Further modelling of scattering in YSO systems taking into account all their components (and not only the disk) would be helpful to test this possibility quantitatively.

Are there other possibilities to understand how the narrow permitted emission lines are formed in edge-on systems? In order to investigate this question, we focus on the Na I resonance lines. In the following paragraphs, we briefly compare the Na I D lines observed in edge-on systems with those seen in other CTTSs and discuss the various possible formation regions for these resonance lines.

4.3.2. Comparison with other CTTSs

The following discussion is based on CTTS high resolution sodium line profiles published by Edwards et al. (1994), Muzerolle et al. (1998), Alencar & Basri (2000), and Alencar & Batalha (2002), so the reader is referred to these papers for a comparison with our data. Since some of the above authors do not present the observed profiles but residuals obtained by subtracting a template photospheric Na I D from the observations, we provide the residuals for program stars HV Tau C and HK Tau C in Fig. 12 after subtracting from the spectra the photospheric lines of the template star LDN 1551-9.

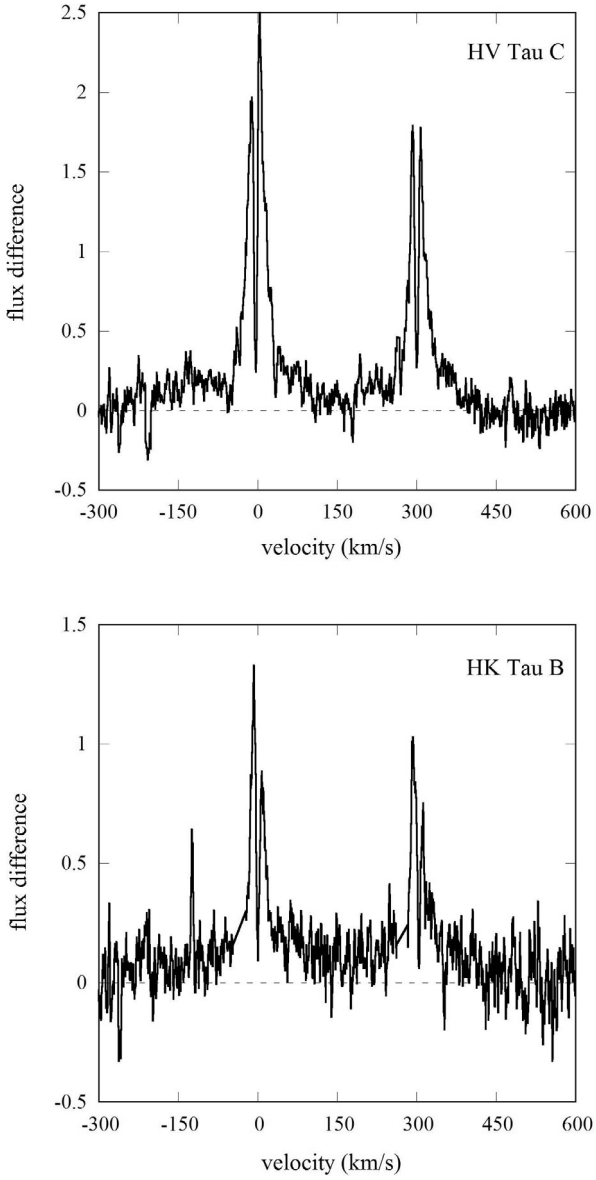

Fig. 12. Residual Na I D lines of HV Tau C and HK Tau B after subtracting template photospheric absorption lines.

The extreme narrowness of the emission peaks is readily apparent from Figs. 10 and 12, while the residuals also display a wide, low flux level pedestal that extends up to about 100 km s^{-1}. An emission deficit in the blue wing of the line is also apparent in HV Tau C. The flux ratio of the blue to red line wings is 89%. Our HH30* spectra are too noisy to allow for a meaningful integration of the flux, and the geocoronal sodium emission disturbs the weak emission line of HK Tau B, thus making it difficult to say whether a similar effect is present.

A comparison with published Na I D reveals both the wealth of profile shapes displayed by these resonance lines in the CTTS class and the almost unique position of edge-on stars in this class. Wide emission peaks are common (e.g., DF Tau, DG Tau, DL Tau), as are prominent blue-displaced absorption components (e.g., DF Tau, DG Tau, DO Tau) and shallow red-displaced absorption components (e.g., AA Tau, DK Tau, DR Tau). The only star in the sample of 27 CTTSs that displays similarly narrow emission peaks is the well-known star TW Hya, the nearby CTTS that is seen almost pole-on (Alencar & Batalha 2002).

The question thus arises whether the narrowness of the Na I D lines is a reliable indication that emission from the edge-on stars is effectively seen pole-on (as in TW Hya) or whether the sodium line-forming region in our stars has properties that would result in an intrinsically narrow line width even at large view angle. To answer this question, we examine in turn the various possible regions for sodium line formation. Three possible regions come to mind: the magnetospheric accretion region, the innermost disk layers, and the inner disk wind region. In theory, these three regions can contribute to line emission from CTTSs, but in recent years attention has focused mainly on the magnetosphere as the main origin of CTTS line emission.

4.3.3. Na I D formation in the magnetospheric region

The current paradigm for CTTSs assumes that permitted emission lines are formed in the magnetospheric region; and detailed models were computed by Muzerolle et al. (2001), who present a grid of Na I D residual profiles computed for various mass accretion rates and magnetosphere properties for a view angle of 60°. These profiles often show an emission peak becoming wider at low flux, and sometimes display shallow red-displaced absorption components. In some cases, the emission peak becomes extremely narrow as observed in our program stars. Interestingly, the Na I D lines of the near pole-on star TW Hya were fitted reasonably well by Alencar & Batalha (2002) using one of these magnetospheric profiles computed for a 60° view angle. One might therefore conclude that the narrowness of sodium emission lines in edge-on stars can readily be understood in the framework of the current magnetospheric accretion paradigm.

One observed fact, however, is not reproduced in the framework of this model. As noted above, the flux in the blue wing of the Na I D residual lines is smaller (by about 10%) than in the red wing of the HV Tau C lines, which in our sample has the best signal-to-noise ratio. The signal-to-noise of our HK Tau B and HH30* spectrograms does not allow for a meaningful integration of the sodium line wings, but visual inspection of Fig. 10 suggests that the same effect is present in the other edge-on stars. This seems to indicate that blue-displaced material absorbs some of the sodium line photons. When carefully studying theoretical emission profiles formed in magnetospheric accretion regions, however, one sees that the situation is *always* reversed; i.e., the red-ward line flux is always smaller than the blue-ward flux, reflecting absorption in the infalling magnetospheric region. We thus conclude that the outflow is likely to play a role in the formation of Na I D at least in HV Tau C and possibly in other edge-on stars.

4.3.4. Na I D formation in the innermost disk region

The innermost regions of irradiated accretion disks reach temperatures in the 2000−3000 K range, where sodium emission

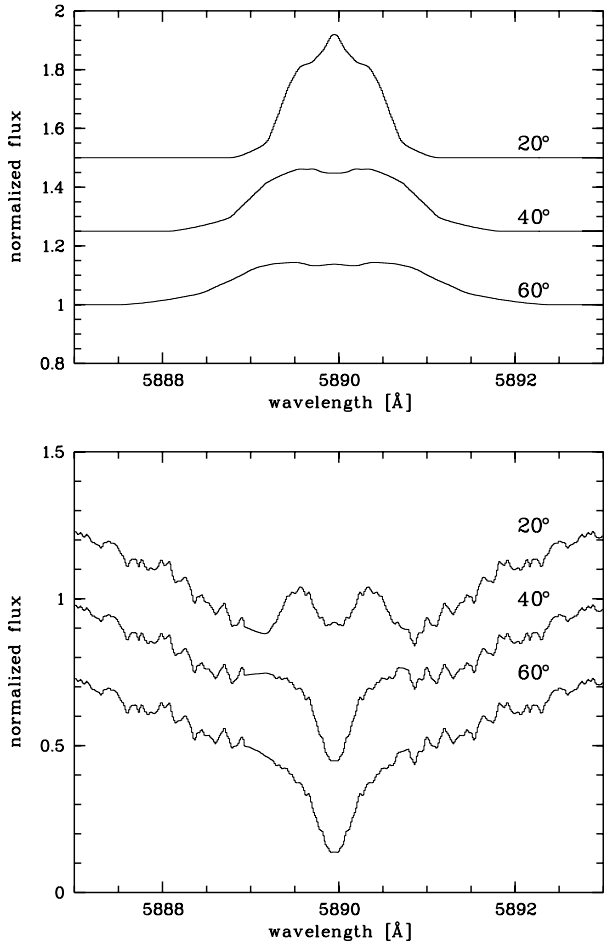

Fig. 13. Na I D1 line profiles formed in an accretion disk seen at different view angles (20°, 40°, and 60°). Panel **a)**: Line residuals as defined in the text. Panel **b)**: the photospheric Na I D1 absorption line is taken into account in the computation.

can occur if the gas density is sufficient. We use a 2D line transfer code developed for investigating ejection/accretion structures (Bertout et al., in preparation) to compute line formation in the inner parts of an α accretion disk with reprocessing taken into account as in Bertout (2000), and found that narrow, doubly-peaked emission lines could be formed in this region, provided the disk is seen close to pole-on. As soon as the view angle becomes larger, the emission lines become wider as expected on the basis of the quasi-Keplerian velocity field present in the disk. Figure 13 presents line profiles originating from the innermost disk region as seen by observers looking at the system from different view angles. The disk parameters are the same as given in Table 6 except for the mass accretion rate, which is larger by a factor of ten. View angles are respectively 20, 40, and 60 degrees. Panel (a) of Fig. 13 shows the residual line emission as defined above, and Panel (b) shows the disk emission when the Na I D1 photospheric background flux is taken into account. Clearly, the extended wings due to disk emission which are seen in the Na I D1 line even at moderate view angles, are not compatible with observations.

In the framework of the (admittedly simple) disk model investigated here, we found that the Na I D line emission from the disk alone is insufficient to explain the observed flux unless the mass-accretion rate is several $10^{-7}\ M_\odot\ \mathrm{yr}^{-1}$, which is not compatible with the moderate veiling observed in edge-on systems. A potential way out of this difficulty is to consider the strong anisotropy of stellar light reprocessing, which would result in a temperature inversion at the disk surface (see, e.g., Malbet & Bertout 1991). It is obvious that such a "chromospheric" disk layer will somewhat increase emission in the optical resonance lines. Thus, more detailed disk models that take surface heating into account in a more accurate way need to be investigated in order to precisely calibrate the line emission expected from accretion disks. It appears, nevertheless, unlikely that strong resonance lines can be entirely formed in the disk at the moderate accretion rates displayed by many CTTSs.

Table 6. Computation parameters for the lines shown in Figs. 14 and 15. The various parameters are defined in the text.

	Model 1	Model 2
$R_{\rm star}$	$2\ R_\odot$	
$M_{\rm star}$	$0.5\ M_\odot$	
$T_{\rm eff}$	3500 K	
$R_{\rm D}^{\rm min}$	$2\ R_{\rm star}$	
$R_{\rm D}^{\rm max}$	1 AU	
$\dot{M}_{\rm D}$	$4\times10^{-8}\ M_\odot\ \mathrm{yr}^{-1}$	
α	10^{-2}	
β	2	0
γ	5×10^{-2}	3×10^{-2}
$T_{\rm jet}$	10^4 K	
$V_{\rm jet}$	$100\ \mathrm{km\ s}^{-1}$	
V_ϕ	$15\ \mathrm{km\ s}^{-1}$	

We thus rule out disk emission alone as a possible explanation of the observed narrow Na I D lines. We note, however, that disk emission contributes to filling up the deep photospheric absorption features (Fig. 13), even at moderate disk accretion rates, and is thus a needed component for explaining the emission lines formed in the disk wind models discussed in the next section.

4.3.5. Na I D formation in the inner disk wind

In the disk wind acceleration region located close to the disk surface, the poloidal velocities are expected to be small, while the toroidal velocities are comparable to the Keplerian velocity of the disk region where the wind is launched (see, e.g., Pesenti et al. 2004). One would thus tend to expect the lines formed there to be wide as soon as the view angle is moderate, similar to the disk case. There is, however, an additional factor to take into account, the acceleration and collimation of the outflow expected to occur within a few AUs. If collimation of the outflow takes place on small scales, it could well be that the range of observed radial velocities could be narrowed even at high inclination angles.

In order to test this possibility, we used our 2D line formation code to compute line profiles emerging from a disk/jet toy model that is set up as follows. The disk is modeled as in the previous paragraph. We then assume that the jet

radial velocity increases as $v \propto r^{\delta}$ from the local sound speed at the inner disk radius to a maximum velocity $V_{\rm jet}$ that is reached at the outside boundary of the computational domain, a sphere of radius 1 AU. For computational simplicity, the rotational velocity component in the jet V_{ϕ} is assumed to be equal to a constant fraction of the Keplerian velocity at the inner disk radius, and the base of the jet is assumed to fill up the full solid angle not occupied by the disk, except for the innermost cylinder between the rotation axis and the inner disk radius, which we take to be hollow. We use a latitude-dependent density law to mimic collimation along the rotation axis. More specifically, we assume that the jet density varies as $\rho(r,\theta) \sim \rho(r,0)\left[1-(\sin\theta/\sin\theta_{\rm D})^{\beta}\right]$ where θ is the angle between the jet axis and the radius vector $\vec{r}$ and where $\theta_{\rm D}$ is the disk's opening angle. The radial variation of density follows from the condition of mass conservation, assuming that the mass-loss rate in the jet is equal to a fraction γ of the disk mass-accretion rate. The jet is assumed to be isothermal with temperature $T_{\rm jet}$. Other parameters of the system are the stellar radius $R_{\rm star}$, the stellar mass $M_{\rm star}$, its effective temperature $T_{\rm eff}$, the disk inner radius $R_{\rm D}^{\rm min}$ and outer radius $R_{\rm D}^{\rm max}$, its mass-accretion rate $\dot{M}_{\rm D}$, and the viscosity parameter α.

Using this toy model, we found that line profiles resembling observed ones were easily produced for system parameters that are typical of CTTSs, and we computed two sets of models, shown in Figs. 14 and 15. The first one is for modest jet collimation ($\beta = 2$) and the second one is uncollimated ($\beta = 0$). Table 6 presents the parameters relevant to the computed sets of profiles. With the modest disk-accretion rate assumed here, the main contribution to Na I line emission comes from the base of the wind. Thus, in accordance with the observations, the fast-moving outer part of the jet does not contribute to the Na I D lines.

We found that the Na I profiles similar to those observed can be explained by a model combining a disk accretion rate in the range $1{-}5 \times 10^{-8}\ M_{\odot}\,{\rm yr}^{-1}$, which are typical values for moderate CTTSs, with a wind expelling a few % of the accreted mass.

Collimation of the wind is found to be of crucial importance in determining the shape of profiles formed in our toy model. Emission profiles formed in a collimated wind (model 1) remain narrow at all view angles, even for the moderate amount of collimation that we used in our toy model. This occurs because the emitting gas is concentrated along the rotation axis so that the range of projected velocities seen by the observer as originating from the emitting volume is narrow. As explained in the previous paragraph, emission from the inner disk layers provides the wide basis seen in the residual profile at 60° view angle in Fig. 14, which fills up partly the photospheric absorption.

In an uncollimated wind (model 2), by contrast, the projected outflow velocities in the observer's direction cover a wider range at all view angles and, together with the underlying disk emission, contribute to the widening of the overall profile. We note the resemblance between the sodium lines observed in HL Tau and the model profiles for 60°. In this uncollimated wind, narrow profiles can be achieved only when disk emission is suppressed, i.e., when the disk is seen close to pole-on.

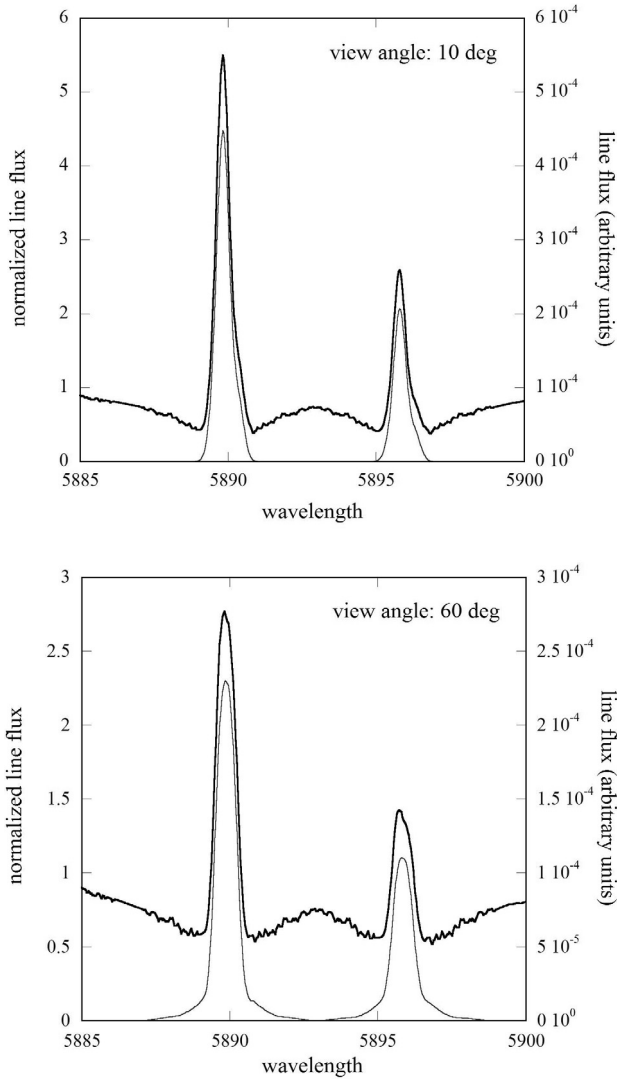

Fig. 14. Na I D line profiles formed in the toy model described in the text. The darker solid line shows the line flux normalized to the continuum in the vicinity of the lines, while the lighter solid line shows the residual line flux once the photospheric contribution is subtracted. Parameters for this computations are those of model 1 in Table 6. In particular, a modest collimation of the wind is assumed here.

To the question we asked ourselves at the beginning of this section we can now answer that there are indeed some disk wind geometries that produce narrow Na I D emission lines for all view angles. In fact, these profiles bear strong resemblances to profiles formed in magnetospheric accretion regions, as the residual profiles shown in Fig. 14 indicate. Both models predict narrow residual profiles with an additional wide basis when seen at 60°. In addition, the wind residual profiles formed in our toy model exhibit a modest flux deficit on the blue side of the lines that is presumably due to self absorption. More specifically, the flux in the blue side of the lines seen is about 80% of the flux in the red line side. As noted earlier, a similar effect is observed in the sodium line residuals of HV Tau C.

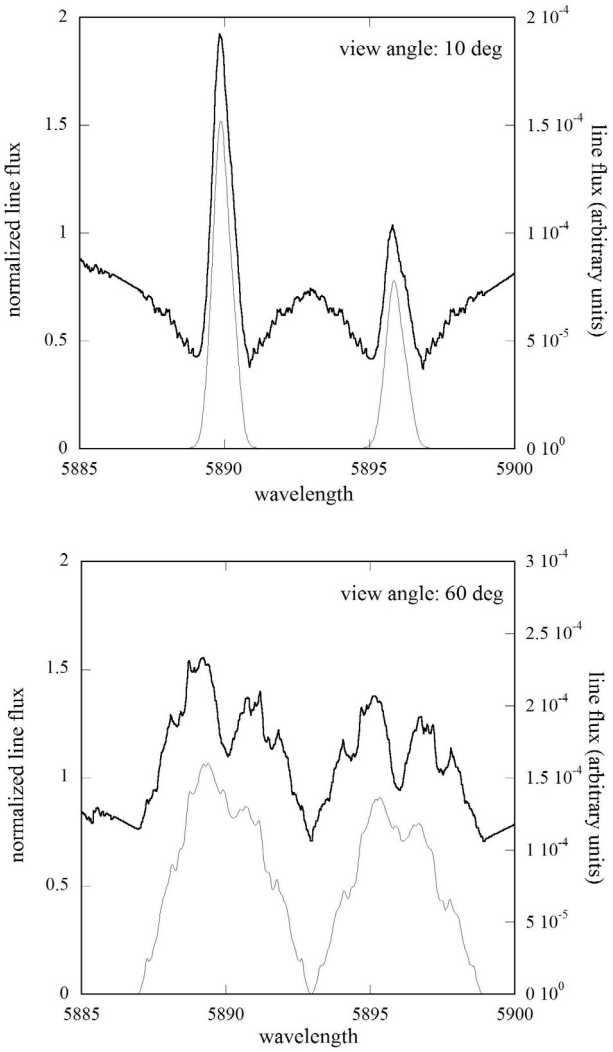

Fig. 15. Same as Fig. 14 but for the parameters of model 2 in Table 6. Here, the disk wind is uncollimated.

There is nevertheless a problem with the idea that the Na I D lines might be formed in such a wind model. Since the view angle hardly affects the profile shape of the computed lines, one should observe many stars with such narrow profiles, if this physical mechanism is the dominant one in sodium line formation. As noted above, this is not the case; among the many CTTSs observed at high spectral resolution, only the edge-on stars and TW Hya were found to exhibit narrow Na I D emission peaks. In many cases, the observed profiles are wide, as seen e.g. for HL Tau in Fig. 10. The same criticism probably applies to the published sodium profiles formed in magnetospheric models, which do not seem able to produce wide emission components even at high inclination.

It could well be, however, that more realistic disk wind models will be able to reproduce different resonance line shapes for the same view angles depending, for example, on the wind collimation degree or the accretion/ejection geometry. In this context, the current lack of physically consistent models for the accretion/ejection region and jet is a real problem for interpreting YSO emission line profiles. The development of realistic models for accretion/ejection structures is under way (e.g., Pesenti et al. 2004) and appears to be the main key to further understanding YSO physics. The results reported here are nevertheless encouraging because they demonstrate that a simple toy model can easily account for the bulk properties of the Na I resonance line emission with a set of parameters relevant to CTTS systems.

5. Conclusions

As pointed out above, our observations have shown that the observed edge-on disks in the Taurus star formation region are actually CTTSs where the line-of-sight to us by chance coincides with the plane of the proto-stellar (and pre-planetary) accretion disk. Thus, our observations provide further support to the current theoretical concepts of low-mass star formation which assume that the CTTSs are pre-main sequence stars surrounded by both cool, dusty accretion disks and remnants of their proto-stellar envelopes. The different amounts of veiling observed and the different jet strengths of the three observed edge-on disks indicate different mass accretion rates of the central T Tauri stars, or possibly different evolutionary stages. But otherwise these stars show no detectable systematic differences from other known CTTSs apart from the different viewing angle. We conclude that all classical T Tauri stars very likely show the morphology of our targets when viewed edge-on. That edge-on T Tauri stars have met with little attention so far is obviously explained by the fact that at the same distance they appear much fainter than their less inclined counterparts. With the new large telescopes and better detectors probably many more of these objects will be found in galactic star formation regions.

For a comparison with theoretical models, edge-on T Tauri stars have the significant advantage that the inclination of the disk and jet systems is known. Because of the high spectral resolution of the UVES spectra and the narrow profiles of the forbidden lines in our edge-on objects, the Hα, He I, and forbidden lines show interesting details that could not be detected in earlier spectra. As described in Sect. 3, our spectra show two different components of line emission, which originate from different regions and under different physical conditions in the T Tauri systems. They also demonstrate beyond any doubt that jet emission contributes not only to forbidden emission but also to permitted lines such as Hα and He I, which suggests that the view angle plays a role in the appearance of CTTS emission lines. In Sect. 4.2, a comparison of Hα equivalent widths in a small sample of Taurus-Auriga CTTSs with known view angles showed that the Hα equivalent widths increase on average with the system's view angle after correcting for the effect of veiling

As discussed above, we conclude that there are two possible ways to interpret the optical light reaching us from the center of these systems: (a) it could be scattered in our direction by matter located along the rotation axis; or (b) it could originate mainly at the base of a disk wind showing some degree of collimation, in which case light scattering occurs in the disk atmosphere as usually assumed. In Sect. 4 we have demonstrated that with this second hypothesis the modeling of the resonance line emission from the disk and the base of the jet can reproduce the observed narrow Na I emission lines of our edge-on

T Tauri stars. However, further modeling of scattering in YSO envelopes and of line formation in realistic disk wind models is needed to make a definitive choice between these conclusions.

Comparing our spectra of the edge-on stars with that of the T Tauri star HL Tau we find similarities as well as marked differences. However, all observed differences are readily explained by the edge-on aspect of our program objects. In view of this result we regard our study as a promising first step towards a thorough investigation of orientation effects in T Tauri spectra.

Acknowledgements. It is a pleasure to thank the ESO Paranal Observatory staff for carrying out for us the service mode observations on which this paper is based. Many thanks also to Sylvie Cabrit and referee Christopher Johns-Krull for carefully reading our manuscript and for making many valuable comments. We are indebted to Jérôme Bouvier for useful comments and for communicating to us his compilation of rotation periods and radial velocities for T Tauri stars. I.A. gratefully acknowledges the award by the French Ministry of Education of a Prix Gay Lussac-Humboldt, which resulted in a very enjoyable stay at the IAP, Paris, in the course of which this work was initiated. I.A. also wishes to thank C.B., and the director and staff of the IAP for their kind hospitality. This joint research project was supported in part by the European Research Training Network "The Origin of Planetary Systems" (PLANETS, Contract Number HPRN-CT-2002-00308).

References

Adams, F. C., Lada, C. J., & Shu, F. H. 1987, ApJ, 312, 788
Alencar, S. H. P., & Basri, G. 2000, AJ, 119, 1881
Alencar, S. H. P., & Batalha, C. 2002, ApJ, 571, 378
André, P., Ward-Thompson, D., & Barsony, M. 1993, ApJ, 406, 122
Appenzeller, I. 1983, Rev. Mex. Astron. Astrofis. 7, 151
Appenzeller, I., Oestreicher, R., & Jankovics, I. 1984, A&A, 141, 108
Basri, G., & Batalha, C. 1990, ApJ, 363, 654
Basri, G., & Bertout, C. 1989, ApJ, 341, 340
Beckwith, S. V. W., Sargent, A. I., Chini, R. S., & Guesten, R. 1990, AJ, 99, 924
Bertout, C. 2000, A&A, 363, 984
Bertout, C., Basri, G., & Bouvier, J. 1988, ApJ, 330, 350
Bertout, C., Robichon, N., & Arenou, F. 1999, A&A, 352, 574
Burrows, C. J., Stapelfeldt, K. R., Watson, A. M., et al. 1996, ApJ, 473, 437
Cabrit, S. 2002, Proceedings of Star Formation and the Physics of Young Stars, held 18–22 September, 2000 in Aussois, France, ed. J. Bouvier, & J.-P. Zahn, EDP Sciences, EAS Publications Ser., 3, 147
Cabrit, S., Edwards, S., Strom, S. E., & Strom, K. M. 1990, ApJ, 354, 687
Cabrit, S., Guilloteau, S., Andre, P., et al. 1996, A&A, 305, 527
Calvet, N., Basri, G., & Kuhi, L. V. 1984, ApJ, 277, 725
Close, L. M., Roddier, F., Northcott, M. J., Roddier, C., & Graves, J. E. 1997, ApJ, 478, 766
Cohen, M., & Jones, B. F. 1987, ApJ, 321, 846
Cohen, M., & Kuhi, L. V. 1979, ApJS, 41, 743
D'Alessio, P., Canto, J., Calvet, N., & Lizano, S. 1998, ApJ, 500, 411
D'Alessio, P., Calvet, N., Hartmann, L., Lizano, S., & Cantó, J. 1999, ApJ, 527, 893
D'Alessio, P., Calvet, N., & Hartmann, L. 2001, ApJ, 553, 321
Duchêne, G., Ménard, F., Stapelfeldt, K., & Duvert, G. 2003, A&A, 400, 559
Edwards, S., Hartigan, P., Ghandour, L., & Andrulis, C. 1994, AJ, 108, 1056
Favata, F., Giardino, G., Micela, G., Sciortino, S., & Damiani, F. 2003, A&A, 403, 187
Feigelson, E. D., & Kriss, G. A. 1983, AJ, 88, 431
Graham, J. A., & Heyer, M. H. 1990, PASP, 102, 972
Hamann, F. 1994, ApJS, 93, 485
Hamann, F., & Persson, S. E. 1992, ApJS, 82, 247
Hartmann, L., Avrett, E., & Edwards, S. 1982, ApJ, 261, 279
Hartmann, L., Calvet, N., Gullbring, E., & D'Alessio, P. 1998, ApJ, 495, 385
Hayashi, M., Ohashi, N., & Miyama, S. M. 1993, ApJ, 418, L71
Henney, W. J., & O'Dell, C. R. 1999, AJ, 118, 2350
Herbig, G. H., & Kameswara Rao, N. 1972, ApJ, 174, 401
Hirth, G. A., Mundt, R., & Solf, J. 1997, A&AS, 126, 437
Kenyon, S. J., Brown, D. I., Tout, C. A., & Berlind, P. 1998, AJ, 115, 2491
Koresko, C. D. 1998, ApJ, 507, L145
Kuhi, L. V. 1964, ApJ, 140, 1409
Kwan, J., & Tademaru, E. 1988, ApJ, 332, L41
Lynden-Bell, D., & Pringle, J. E. 1974, MNRAS, 168, 603
Magazzu, A., & Martin, E. L. 1994, A&A, 287, 571
Malbet, F., & Bertout, C. 1991, ApJ, 383, 814
Ménard, F., & Bertout, C. 2002, Proceedings of Star Formation and the Physics of Young Stars, held 18–22 September, 2000 in Aussois, France, ed. J. Bouvier & J.-P. Zahn (EDP Sciences, Les Ulis), EAS Publications Ser., 3, 183
Monin, J.-L., & Bouvier, J. 2000, A&A, 356, L75
Mundt, R. 1984, ApJ, 280, 749
Mundt, R., & Fried, J. W. 1983, ApJ, 274, L83
Mundt, R., Brugel, E. W., & Buehrke, T. 1987, ApJ, 319, 275
Mundt, R., Buehrke, T., Solf, J., Ray, T. P., & Raga, A. C. 1990, A&A, 232, 37
Muzerolle, J., Hartmann, L., & Calvet, N. 1998, AJ, 116, 455
Muzerolle, J., Calvet, N., & Hartmann, L. 2001, ApJ, 550, 944
Pesenti, N., Dougados, C., Cabrit, S., et al. 2004, A&A, 416, L9
Reipurth, B. 1999, A general catalogue of Herbig-Haro objects, 2nd edition, `http://casa.colorado.edu/hhcat/`
Reipurth, B., Heathcote, S., Roth, M., Noriega-Crespo, A., & Raga, A. C. 1993, ApJ, 408, L49
Simon, M., Chen, W. P., Howell, R. R., Benson, J. A., & Slowik, D. 1992, ApJ, 384, 212
Stahl, O., Kaufer, A., & Tubbesing, S. 1999, Optical and Infrared Spectroscopy of Circumstellar Matter, in ASP Conf. Ser. 188, 331
Stapelfeldt, K. R., Burrows, C. J., Krist, J. E., et al. 1995, ApJ, 449, 888
Stapelfeldt, K. R., Krist, J. E., Menard, F., et al. 1998, ApJ, 502, L65
Stapelfeldt, K. R., Ménard, F., Watson, A. M., et al. 2003, ApJ, 589, 410
Strom, K. M., Strom, S. E., Edwards, S., Cabrit, S., & Skrutskie, M. F. 1989, AJ, 97, 1451
Takami, M., Bailey, J., & Chrysostomou, A. 2003, A&A, 397, 675
Watson, A. M., & Stapelfeldt, K. R. 2004, ApJ, 602, 860
White, R. J., & Hillenbrand, L. A. 2004, ApJ, 616, 998
Woitas, J., & Leinert, C. 1998, A&A, 338, 122
Wood, K., Kenyon, S. J., Whitney, B., & Turnbull, M. 1998, ApJ, 497, 404
Yorke, H. W., & Bodenheimer, P. 1999, ApJ, 525, 330